A Study on the Physical Properties of the Newly Calculated Phases of Cu–Al–Be Alloys by *ab initio* Calculations

C. Soykan

Ahi Evran University, Vocational School of Health Services, Kırşehir, Turkey

(Received January 28, 2019; revised version April 17, 2019; in final form July 22, 2019)

Total energy calculations based on density functional theory were performed to investigate the physical properties for the austenitic $L2_1$ and newly calculated martensitic phases of the Cu_2 AlBe shape memory alloy. When the total energy of all the phases versus the volume data are fitted to the Birch–Murnaghan equation of state, it is seen that the stable martensitic NM, 3M, 5M, and 7M phases of the alloy can exist. The lowest energetic phase was determined as tetragonal non-modulated NM structure. When we compare the energy of the newly calculated martensitic phases to the thermal fluctuation energy barriers (criteria as $(3k_BT)/2$ meV/atom is taken), we are confident that the energy difference between 5M, 7M, and 9R phases and the NM phase is large enough to overcome the thermal energy barrier. Moreover, it has been observed that the calculated elastic constants of austenitic $L2_1$ and martensitic NM, 3M, 5M, 7M, and 9R phases provide all the mechanical stability conditions determined according to crystal structure symmetries. We consider that the phases that exceed the thermal energy barriers and satisfy the mechanical stability conditions can exist at a stable energy level. When the partial electronic density of states (pDOS) of the austenitic and martensitic phases are analyzed, it is seen that the most contribution to the electronic density of states comes from Cu t_{2g} and Cu e_g states. In addition, it is seen that the contributions to the electronic density of state from not only s, p, t_{2g} and e_g states of Al and Be atoms but also s and p states of Cu atom have been observed extremely small quantity in the all austenitic and martensitic phases. On the other hand, the t_{2g}, and e_g states of Cu atoms dominate in the electronic nature of the Cu_2AlBe shape memory alloy. Cu_2AlBe shape memory alloy is a non-magnetic material since all phases of spin-up and spin-down are all symmetrical.

DOI: 10.12693/APhysPolA.136.411

PACS/topics: shape memory alloys, Cu–Al–Be alloys, structural properties, mechanical properties, electronic band structures.

1. Introduction

Many different types of alloys have been developed as alternatives to Ni–Ti alloys, which is the most common conventional shape memory alloy (SMA). While Ti–Ni alloys have a limited range of martensitic transformation within 200–300 K range [1, 2], Cu–Al based SMAs have a wider range of martensitic transformation temperatures such as 77–473 K [3–5]. However, different triple Cu–Al based alloys such as Cu–Al–Mn [5, 6], Cu–Al–Be [7, 8] and Cu–Al–Ni [9–11] have been reported to have better mechanical behavior. In addition, the most important factors in favor of Cu-based alloys include lightness, successful shape memory effect, affordable price, very good damping capacity, and good characteristics. Due to these advantageous properties, Cu-based alloys have the potential to be used in application fields such as automotive, aerospace industries, and as sensors and actuators for health monitoring and microelectromechanical devices.

It has been observed that Cu–Al–Be SMAs exhibit martensitic phase transition from $L2_1$ (austenitic) phase to 18R or 18R to 6R phase depending on the strain [12]. Due to this martensitic phase transition, the changing properties make the Cu-based alloy attractive for damping applications. Pseudo-elastic behavior is a feature that SMAs can exhibit. Pseudo-elastic behavior in Cu-based alloys is dependent on the stress that occurs from the austenitic DO_3 (or $L2_1$) phase to the 18R martensitic phase during the martensitic phase transition. The stress required for martensitic transformation is higher than that required for recycling the austenitic phase, which leads to hysteresis. In recent studies, it has been reported that the 18R martensitic phase exhibits structural distortion under tensile stress [8]. In addition, the 18R–6R pseudo-elasticity cycle has two distinguishable features [12]. The stress required to induce the martensitic 6R phase is almost independent of the temperature, and the hysteresis at these transitions is considerably greater than the transition temperature. Considering these properties, the hysteresis that occurs in the martensitic phase transitions is very important to develop damping applications of alloys [7, 12, 13].

Tensile tests carried out at a slower cross rate of 18R martensitic transformation for the Cu–Al–Be alloy show that the hysteresis is temperature and strain dependent. However, it has been determined that the entropy changes from the structural deterioration during this transformation is fifty times smaller than from

corresponding author; e-mail: cengiz.soykan@ahievran.edu.tr

austenitic $L2_1$ phase to 18R martensitic phase transition shift entropy change [8]. Unlike most of the previously reported martensitic transitions, structural distortions in the martensitic phases during phase transitions in Cu-based shape memory alloys can show a hysteresis that is not clearly noticeable in experimental solubility.

Determining the elastic constants of materials accurately is crucial firstly from a scientific standpoint because it allows an analysis of the microstructural parameters of the material. Secondly, for designing new engineering applications, elastic constant data are used as critical input. The most general experimental methods for determining elastic constants can be classified as static and dynamic. Although static methods such as stretching, compression, twisting can measure elastic constants well, the dynamic methods have many advantages for calculating elastic constants. Young's modulus of Cu–Al–Be alloy was investigated by using a dynamic method, impulse excitation technique (EIT) [14]. In our study, the elastic constants can be successfully calculated theoretically by using the linear deformation method (LD) and the linear response method (LR) applied within the elastic limit. The phase transformations that occur in the materials can change the electronic properties of the material as well. Changes in the electronic structure of the Cu–Al–Be alloy in the transitions between irregular austenitic A2, regular austenitic DO_3 (or $L2_1$), and 18R martensitic phases were studied by electron energy loss spectrometry (EELS) and after the martensitic transition, a charge of approximately 0.17 electron/atom remained in the Cu $3d$ state [15]. Furthermore, it was not observed that transfer of charge occurred from martensitic to austenitic or between regular-irregular austenitic phases [15]. From this point of view, it can be seen that the change of charge can give important information about whether the crystallographic structure of the material has changed or not.

To summarize briefly the results obtained from the present studies, firstly, it is observed that hysteresis can also occur not only for the phase transition from the parent phase to the martensitic phase ($L2_1$ to 18R) but also between martensitic phases (18R to 6R) in the Cu–Al–Be alloys [7, 8, 12, 13]. Secondly, it has been reported that not only unexpected mechanical behavior occurs due to structural deterioration during phase transitions but also in this case hysteresis occurring in Cu-based alloys cannot be observed experimentally [8]. From this point of view, the determination of the mechanical stability state of the alloy is important depending on the stability conditions of the cubic ($L2_1$), tetragonal (NM), and orthorhombic phases (3M, 5M, 7M, and 9R) in the Cu_2AlBe SMA. This is because, understanding the mechanical stability of the solid-state lies in the formulation of stability criteria, a set of conditions that determine the critical level of external stress or internal strains at which a homogeneous lattice without any defects becomes structurally unstable. Mechanical stability is one of the most central issues in the analysis of structural reactions such as the formation, growth, single crystalline, or polycrystalline form of a crystal. Accordingly, lattice stability is one of the most fundamental issues in the flexibility and stability of the crystal phase [16, 17]. In order to determine the mechanical stability of the calculated austenitic ($L2_1$) and martensitic (NM, 3M, 5M, 7M, and 9R) phases in Cu–Al–Be SMA, it has been investigated whether it provides the mechanical stability conditions. These mechanical stability conditions are determined by the stability criteria based on the symmetries of the crystal structures. Correspondingly, the provision of mechanical stability will be a reference point for supporting the stability of newly calculated crystal lattice. Thirdly, it is understood that electronic charge exchange can be regarded as an indication of phase transitions in SMAs [15]. In the light of all these informations, the presence of stable NM (non-modulated), 3M, 5M, and 7M martensitic phases were investigated in this study in addition to previously observed DO_3 (or $L2_1$) austenitic and 18R-6R martensitic phases. The structural, mechanical, and electronic properties of the stable state are also calculated to assess the potential of these phases in their application areas. In our study the results obtained not only are compatible with the previous data for the austenitic $L2_1$ and martensitic 9R phases but also will provide significant contributions to the literatures physical properties of the Cu–Al–Be alloy, in the theoretically conjectured and investigated NM, 3M, 5M, and 7M phases.

2. Computational details

In this study, *ab initio* simulation calculations based on the DFT were performed using the potential of the projector augmented wave (PAW) to solve the Kohn–Sham equations [18–20]. Total energy calculations were performed using the Vienna *ab initio* simulation package (VASP) [21–25]. The effects of electronic exchange and correlation functions are considered with using the generalized gradient approximation (GGA) developed by Burke, Perdew, and Ernzerhof [26]. In our calculations, kinetic energy cut-off values for $L2_1$ austenitic, NM, 3M, 5M, 7M, and 9R martensitic structures were determined to be 600 eV. The energy convergence criterion of the electronic self-consistency was chosen as 10^{-8} eV/atom [27]. The Brillouin zone integrations were carried out by the Monkhorst–Pack special points mesh with a grid size of $16 \times 16 \times 16$ (for austenitic $L2_1$), $12 \times 12 \times 10$ (for martensitic NM), $10 \times 2 \times 8$ (for martensitic 3M, 5M, and 7M) and $12 \times 12 \times 10$ (for martensitic 9R) for the all phases in the Cu_2AlBe alloy [28]. The contribution of valence electrons is influential in determining the electronic properties of Cu–Al–Be alloys. The valence electron configurations for Cu, Al, and Be atoms are $3d^{10}4s^1$, $3s^23p^1$, and $2s^2$, respectively. To determine the electronic behavior of the material, the density of electronic states (DOS) was calculated using the tetrahedron method involving the Bloch corrections. In the DOS calculations, the k-mesh numbers are increased

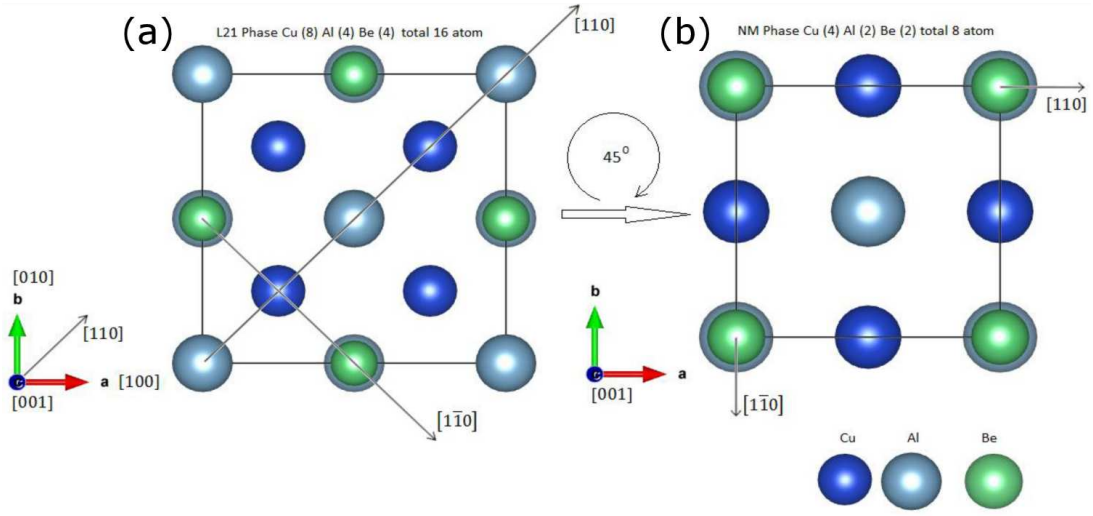

Fig. 1. (a) The illustration of cubic $L2_1$ Heusler phase of Cu_2AlBe SMA. (b) Reduced tetragonal bct nonmodulated (NM) cell of Cu_2AlBe shape memory alloy. Blue, cyan, and green spheres represent Cu, Al, and Be atoms in the pictures, respectively.

to $22 \times 22 \times 22$ (for cubic $L2_1$ phase), $16 \times 16 \times 14$ (for martensitic NM phase), $16 \times 8 \times 14$ (for 3M–5M phases), and $12 \times 4 \times 10$ (for 7M–9R phases). The austenitic cubic $L2_1$ structure has a unit cell of 16 atoms. The unit cell of the tetragonal NM structure also contains 8 atoms.

The 5M modulated crystal structure designed for prototype Ni_2MnGa magnetic SMA (MSMA) has been used to create modulated martensitic super cells for Cu–Al–Be SMA [29]. As given in Fig. 1, to create modulated martensitic super cells of Cu_2AlBe alloy, we used a body-centered tetragonal (bct) primitive cell obtained from the cubic austenitic $L2_1$ structure (from Fig. 1a to b). This primitive cell forms the crystal structure of the non-modulated (NM) martensite phase. In the next step, 3M, 5M, 7M, and 9R structures were created by shifting in non-modulated NM bct primitive cell in the direction of [110] in three, five, seven, and nine atomic planes, respectively. Finally, all atoms are displaced with the same phase according to the acoustic character of the static wave of modulation. In this way, the supercell with modulation resembles as close as possible the experimentally observed structure for Ni_2MnGa single crystals [30]. For example, the relationship between the lattice parameters of the orthorhombic 5M structure consisting of 40 atoms and the cubic $L2_1$ lattice parameter is as follows: $a_{5M} = a_{L2_1}/\sqrt{2}$, $b_{5M} = 5a_{L2_1}/\sqrt{2}$ ve $a_{5M} = a_{L2_1}$ [29]. Martensitic structures with 3M, 5M, 7M, and 9R modulated were periodically iterated 3, 5, 7, and 9 times in the direction of [110], respectively, and orthorhombic super cells with 24, 40, 56, and 72 atoms respectively composed of tetragonal crystallographic units were formed.

The method of forming the martensitic super cells is schematically shown in Fig. 2. Firstly, the structural relaxation is performed with respect to the ionic positions, the shape, and the volume of the supercell. After obtaining the volume at which the energy is minimum, the material is re-relaxed at this volume by changing the shape, volume, and ionic positions at the same time in order to get forces on each atom to be nearly zero. Self-consistent calculations have been terminated when the pressure on the crystal system is approximately 0 kbar and the total force applied on each atom reaches approximately 0.01 eV/Å. When the specified criteria are satisfied, the structural configuration with the lowest energy of the crystal structure is obtained. In the second step, the mechanical properties such as the bulk modulus and the derivative of the bulk modulus are calculated using these equilibrium state structures as reference zero strain state. In the equation of state calculations, the total energy of the crystal structure with the lowest energy determined for each size of unit cell (obtained by increasing and decreasing the volume up to 5%) by fixing the volume of the unit cell and allowing the displacements of the ions until eliminating the forces on them through ionic optimization. This method was repeated for each case by increasing and decreasing the volume of the crystal structure by 5% and a data set was formed by obtaining the total energy for each volume. Note that all results refer to as state at $T = 0$ K without external stress. The total energies of the crystal structure of its volume calculated so as to decide the lattice constants and bulk modulus B_0 (GPa) and its pressure derivative B' by fitting the data to the Birch–Murnaghan equation of states (EoS):

$$E(V) = E_0 + \frac{9}{16} V_0 B_0 \left\{ \left[\left(\frac{V_0}{V} \right)^{\frac{2}{3}} - 1 \right]^3 B_0' + \left[\left(\frac{V_0}{V} \right)^{\frac{2}{3}} - 1 \right]^2 \left[6 - 4 \left(\frac{V_0}{V} \right)^{\frac{2}{3}} \right] \right\}, \quad (1)$$

where E_0, V_0, B_0, and $B^{'}$ are defined as the total energy, equilibrium volume, bulk modulus, and its pressure derivative at the zero pressure, respectively. In order to better understand the mechanical behavior of the material, anisotropic behavior needs to be addressed as well. Hence, we calculate the elastic constants of these new crystal structures, by applying proper linear elastic deformations to the unit cell of the cubic $L2_1$ austenitic structure. The deformation parameters of the three different deformations were selected as $\delta = \pm 0.03, \pm 0.02, \pm 0.01$.

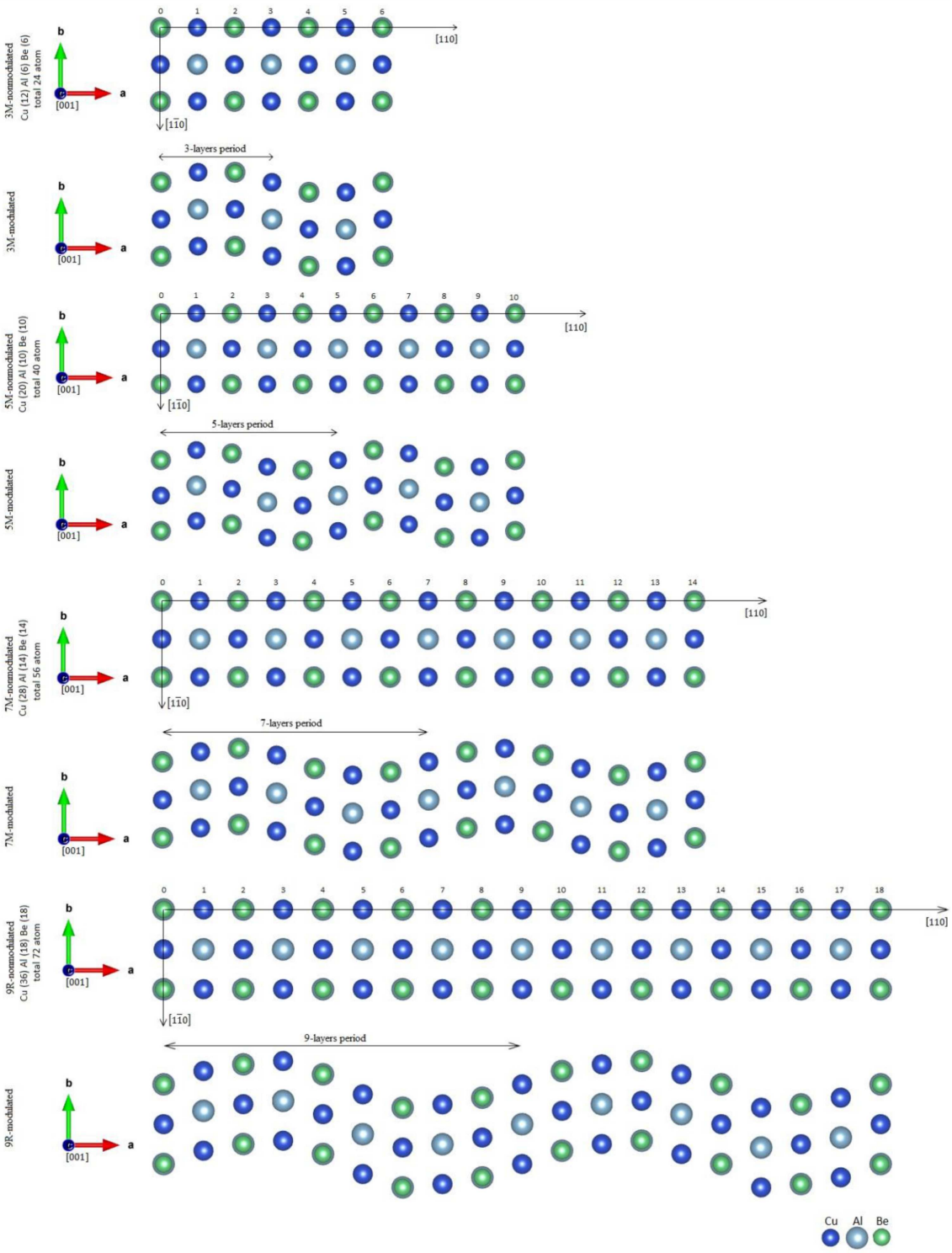

Fig. 2. Modulated martensitic structures of Cu_2AlBe Heusler alloy in the 3M, 5M, 7M, and 9R phases shown schematically: projection of all modulated martensitic phases on the (001) plane (top view).

In this way, C_{11}, C_{12}, C_{44} and bulk modulus B elastic constants have been calculated [31]. The number of elastic constants of martensitic phases is more than six. For this reason, the elastic constants of martensitic phases are calculated by used linear response calculation method (LR), which based on the determination of Hessian matrices [31]. Electronic DOS calculations has also been made to determine the electronic properties of the alloy. In addition, partial electronic density of state (pDOS) calculations were performed to investigate the contributions of Cu, Al, and Be atoms to the electron density of the material, and this distribution of the contributions with respect to the atoms was investigated.

3. Results and discussion

3.1. Structural properties of alloys

The calculated lattice constant of the $L2_1$ phase is 5.712 Å and the corresponding volume of the unit cell is 186.36 Å^3. The calculated lattice constant is in reasonable agreement with the experimental lattice constant, which is reported to in the range of 5.825 Å and 5.963 Å [3, 32]. Together with the $L2_1$ phase, there are experimental and theoretical results from previous works on the 9R phase. The lattice constants a, b, c, of the martensitic 9R structure were also calculated as 4.784 Å, 5.319 Å, and 3.840 Å in our work. The calculated lattice constants of the 9R martensitic phase are consistent with the experimental results [3, 32]. Furthermore, the bulk modulus of the martensitic 9R phase was determined to be 120.4386 GPa and the pressure derivative of the bulk module as 4.4603. The calculated values for cubic austenitic $L2_1$ lattice constants ($a = b = c$) deviated by 4% and 1.9% off from the experimental studies [3, 32].

TABLE I

The calculated lattice parameters a (Å), b (Å) and c (Å) bulk modulus B_0 (GPa) and its pressure derivative B' in the all phases of Cu_2AlBe shape memory alloy.

Structure	Method	Structural properties					
		a [Å]	b [Å]	c [Å]	B [GPa]	B'	Refs.
$L2_1$	our calc.	5.712	5.712	5.712	128.454	4.406	
	exp.	5.963	5.963	5.963			[3]
		5.825	5.825	5.825			[32]
NM	our calc.	4.048	4.048	5.682	129.000	4.353	
3M	our calc.	3.929	4.178	5.885	125.659	4.5193	
5M	our calc.	4.361	4.659	5.212	124.417	4.450	
7M	our calc.	3.956	5.238	4.610	119.911	4.585	
9R	our calc.	4.784	5.319	3.839	120.438	4.460	
	exp.	4.390	5.250	3.830			[3]
		4.460	5.220	12.750			[32]

Ref. [32]. The lattice constants are given without standardization since the material studied by Moreau is polycrystalline (the grain size is given about 50 to 80 μm by Moreau and the unit cell parameters of 18R martensitic measured $a = 0.466$ nm, $b = 0.522$ nm, $c = 1.275$ nm and $\beta = 83.3°$ by using X-ray diffraction patterns)

The first lattice constant a of orthorhombic martensitic 9R phase deviated by 8.9% and 7.2% off from the experimental studies [3, 32]. The second lattice constant b also deviated by 1.3% and 1.9% off from the experimental studies [3, 32]. The third lattice constant c is highly consistent with the experimental study [3]. The deviation rate is only 0.2% [3]. However, since the lattice constant of the experimental study given in Ref. [32] is given without standardizing, it will not be correct to make a comparison. In addition, to the best of our knowledge, there are no experimental and theoretical studies for bulk modulus and its pressure derivative that we can compare our results for austenitic ($L2_1$) and martensitic (NM, 3M, 5M, 7M, and 9R) phases with. Besides, to the best of our knowledge, there are no experimental and theoretical studies related to the lattice constants of newly calculated martensitic (NM, 3M, 5M, 7M, and 9R) phases. The determined structural properties such as lattice constants a, b, c, the mechanical properties, bulk modulus B, and its pressure derivative $B^{'}$ are given in Table I for austenitic $L2_1$ and all martensitic phases.

Experimental studies have shown that the austenitic cubic $L2_1$ structure, which is known as the main stable phase of the Cu_2AlBe alloy, undergoes a phase transformation from 18R and/or 18R to 6R modulated structures depending on the strain [12]. Moreover, the 18R martensitic phase was reported to undergo structural deformation under tensile stress [8]. This result suggests that hysteresis may also occur in the case of phase transitions occurring between martensitic phases [8]. This shows how important it is to investigate the existence of different martensitic phases that may be possible to take advantage of some applications of Cu–Al–Be alloys. From this point of view, the presence of martensitic phases not previously reported has been particularly investigated in this study. The fit results of the total energy value calculated per molecule for all phases to the Birch–Murnaghan EoS are given in Fig. 3.

As shown in Fig. 3, the total energies and the lattice constants, bulk modulus and its pressure derivative corresponding to different volumes per molecule of cubic $L2_1$, tetragonal NM, orthorhombic 3M, 5M, 7M, and 9R crystal structures, by fitting to a third order Birch–Murnaghan equation of state, have been calculated theoretically. The calculated structural parameters are listed in Table I. The lattice constants of tetragonal non-modulated NM phase are calculated as $a = b = 4.048$ Å and $c = 5.682$ Å. Furthermore, the volume V_0, bulk modulus B_0, and its pressure derivative $B^{'}$ corresponding to the minimum energy are calculated as 46.565 Å^3/molecule, 129 GPa, and 4.353, respectively. The energy of the non-modulated tetragonal NM phase is about 2.16 meV/molecule smaller than the cubic phase ($L2_1$) closest to itself. This indicates that the NM phase is a lower temperature phase. To the best of our knowledge, no literature has been found on the experimental and theoretical work that we can compare the structural,

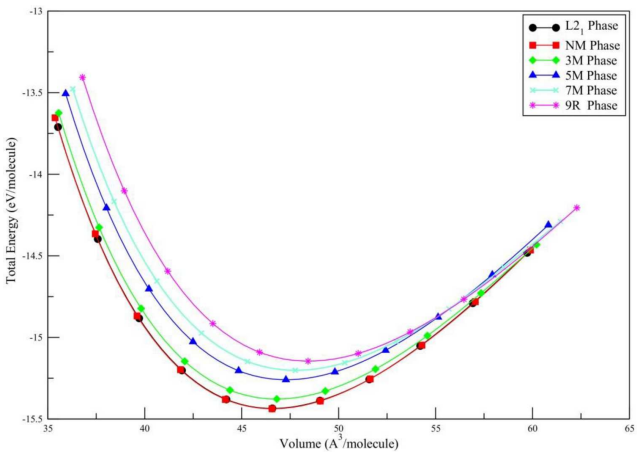

Fig. 3. The equation of state data for $L2_1$, NM, 3M, 5M, 7M, and 9R phases. They are fitted to the 3rd order Birch–Murnaghan equation of state. The total energy values in here are expressed as a function of volume per molecule in the Cu_2AlBe SMA.

mechanical, and electronic properties of the martensitic NM, 3M, 5M, and 7M phases with. For this reason, as given in Fig. 3 not only the new phases calculated according to the Birch–Murhangan state equation have a distribution corresponding to the minimum energy, but also the energy differences between the phases must be evaluated in terms of thermal fluctuation energy. When we consider a thermodynamic system at an absolute temperature T, the average thermal energy carried by each microscopic degree of freedom in the system is about of magnitude k_BT. At room temperature, the value of this thermal energy $k_BT/2$ is approximately 0.012926 eV. As there are three degrees of freedom per atom, corresponding to the three spatial directions, which means a thermal energy of $3k_BT/2$ per atom, this value is approximately 0.03878 eV/atom (or 38.78 meV/atom).

From this point of view, we examine the minimum energy states of the phases; the energy difference between $L2_1$ and NM phases corresponds to about 0.54 meV/atom. This energy value is considerably smaller than the average thermal fluctuation energy of 38.78 meV/atom and the difference of energy between these phases is within thermal fluctuation limits. In the case of the lowest energy of the orthorhombic 3M phase, the lattice constants of phase are calculated as $a = 3.929$ Å, $a = 4.178$ Å, and $c = 5.885$ Å. Structural properties such as bulk modulus and its pressure derivative are also given in Table I. The energy difference between the lowest energy tetragonal NM phase and the orthorhombic 3M phase is estimated to be approximately 14.92 meV/atom. This difference in energy is about half of the thermal energy (38.78 meV/atom). From this, the transition from the NM or $L2_1$ phase to the martensitic 3M phase can be instantaneously induced by thermal energy, or the thermal energy barrier cannot be exceeded. On the other hand, the energy difference between the minimum energies of the martensitic 5M and 7M phases and the minimum energy of the NM phase was calculated to be 44.47 meV/atom and 58.89 meV/atom, respectively. These energy differences are greater than the thermal fluctuation energy value. Thus, a higher energy phase than the low energy phase can be passed over the thermal energy barrier and stable high energy phases can exist. Finally, the difference between the orthorhombic 9R phase and the martensitic NM phase with the lowest energies is calculated to be 72.97 meV/atom. This energy is about twice as much as the thermal fluctuation energy. Considering these results, since the ground state energies of the non-modulated NM and modulated 3M phases have sub energy below the thermal fluctuation energy barrier per atom, their formations can be instantaneously induced by the transported thermal energy. However, the energy differences of the 5M, 7M, and 9R martensitic phases are large enough to exceed the thermal energy barrier. As shown in the Birch–Murnaghan equation of state (given in Fig. 3), the stability of these phases can be mentioned.

3.2. Mechanical properties of alloys

Here we describe the results for the anisotropic elastic properties of different polymorphs of Cu_2AlBe to address the mechanical stability and the effects of martensitic phase transformations on anisotropic mechanical properties. We first investigate the elastic constants for the cubic $L2_1$ austenitic phase of Cu_2AlBe. The elastic constants are obtained by applying three different deformations (volume preserving deformations are used for pure and tetragonal shear coefficients) for cubic $L2_1$ structure. The austenitic $L2_1$ phase has three independent elastic constants. These elastic constants are the bulk modulus $B = (C_{11} + 2C_{12})/3$, tetragonal shear moduli $C' = (C_{11} - C_{12})/2$, and pure shear moduli C_{44}. In our calculations, for each type of lattice deformation, strain parameter δ varies from -0.03 to 0.03 in steps of 0.01 to get the data yielding the strain energy as a function of strain. The deformation energy per unit volume versus strain δ^2 curve gives the corresponding elastic constants from this data. Our calculated bulk modulus and two shear moduli values are compatible with previous experimental studies [33]. The three independent anisotropic elastic constants C_{11}, C_{12}, C_{44} are determined from B_0, C'.

The number of independent elastic constants of martensitic phases (NM, 3M, 5M, 7M, and 9R) is more than three. Depending on the tetragonal symmetry, the number of independent elastic constants of the NM phase is reduced to six. The other martensitic phases with orthorhombic symmetry (3M, 5M, 7M, and 9R) have nine independent elastic constants. For the nonmodulated and modulated structures the elastic constants are calculated by using a LR calculation method, which is based on the determination of Hessian matrices [31]. In addition, both the linear deformation method (LD) and the LR method were used to calculate the elastic constants for the $L2_1$ phase. The values of C_{11}, C_{12}, and C_{44}

TABLE II

The elastic constants C_{ij} (GPa), bulk modulus B_0 (GPa) and tetragonal shear elastic constants $C^{'}$ (GPa) of Cu_2AlBe material in the austenitic and martensitic phases, compared with available experiment and previous theoretical studies

	Structure	Method		Elastic constants C_{ij} [GPa]											Refs.
				C_{11}	C_{12}	C_{13}	C_{22}	C_{23}	C_{33}	C_{44}	C_{55}	C_{66}	B	$C^{'}$	
aus. phase	$L2_1$	our calc.	LR	157.079	109.335					98.056			125.249	23.872	
			LD	145.884	115.699					119.502			125.761	15.092	
		exp.		141.600	94.200					127.400			110.000	23.700	[33]
martensitic phases	NM	our calc.	LR	248.867	46.282	105.162			186.802	2.864		108.017	133.083		
	3M	our calc.	LR	199.753	47.606	115.075	240.689	91.770	190.198	32.164	97.025	109.733	126.616		
	5M	our calc.	LR	170.124	106.769	92.817	183.483	69.527	200.873	69.037	61.952	47.096	121.412		
	7M	our calc.	LR	91.514	59.685	24.273	79.379	40.403	45.115	66.692	39.276	73.612	51.637		
	9R	our calc.	LR	97.079	12.750	37.918	125.322	29.842	91.307	68.515	10.208	50.011	52.748		

calculated by using linear deformation show a deviation of 3%, 22%, and 6%, respectively from the experimental studies. When the results obtained by linear deformation are evaluated, the C_{11}, and C_{44} elastic constants are very compatible with the experimental results, whereas the deviation of C_{12} elastic constant is higher than the others. The deviations observed in C_{11}, C_{12}, and C_{44} elastic constants calculated by the second method LR are 10%, 15%, and 22% respectively, when compared to the experimental results. To best of our knowledge, there are no experimental and theoretical studies to compare the calculated elastic constants for the other five martensitic phases (NM, 3M, 5M, 7M, and 9R). The elastic constants for five martensitic phases (NM, 3M, 5M, 7M, and 9R) are calculated for the first time in this study. The calculated elastic constants for all phases of Cu_2AlBe and the available experimental results are given in Table II.

When the previous studies are examined, it is observed that hysteresis might also occur not only for the phase transition from the parent phase to the martensitic phase ($L2_1$ to 18R) but also between the martensitic phases (18R to 6R) in the Cu–Al–Be alloys [7, 8, 2, 13]. Furthermore, it has been reported that not only unexpected mechanical behavior occurs due to structural deterioration during phase transitions but also in this case hysteresis occurring in Cu-based alloys cannot be observed experimentally [8]. The conditions for mechanical stability in a crystal structure follow from the requirement that upon a general strain deformation, the change in the total energy and all elastic constants (C_{ij}) must be positive. Mathematically necessary and sufficient stability conditions for a crystal system to be mechanically stable can be listed as follows [17]:

- The matrix C_{ij} is definite positive;
- All eigenvalues of C_{ij} are positive;
- Sylvester's criterion must be provided;
- An arbitrary set of minors of C are all positive.

The four possible formulations are called the Born elastic stability conditions for an unstressed crystal system. They are valid regardless of the symmetry of the crystal and are not linear [17].

In order to investigate the mechanical stability in the austenitic and martensitic phases of the Cu–Al–Be SMA, firstly, we review the mechanical stability conditions of the cubic, tetragonal, orthorhombic symmetries, so as to further verify our calculated results for all elastic constants (C_{ij}). The necessary and sufficient stability conditions are given in Table III for the cubic, tetragonal, and orthorhombic crystal symmetries.

The first calculated cubic crystal system is called austenitic $L2_1$. The constraints and restrictions are given in the first row of Table III so that the lattice can be mechanically stable. When viewed with respect to the elastic constants of the cubic $L2_1$ phase, in our results, C_{11}, C_{12}, and C_{44} are 157.079 GPa, 109.335 GPa, and 98.056 GPa, respectively. Besides, the bulk modulus B_0 is 125.249 GPa, and thus, the condition $C_{12} < B_0 < C_{11}$ is satisfied.

The second calculated crystal structure is the martensitic tetragonal NM phase. The stability requirements necessary for a tetragonal crystal to be mechanically stable after applied homogeneous elastic deformation are given in the second row of Table III. All elastic constants of the tetragonal phase are positive as seen in Table II. The restrictions criteria $(C_{11} - C_{12})$, $(C_{11} + C_{33} - 2C_{13})$, and $(2C_{11} + 2C_{12} + 4C_{13} + C_{33})$ are equal to 202.585, 225.261, and 1197.75 GPa, respectively. The bulk modulus B_0 value can be calculated as follows using the elastic constants of the crystal system as given in Ref. [36]:

$$B_0 = \frac{1}{9}\left(C_{11} + C_{22} + C_{33} + 2C_{12} + 2C_{13} + 2C_{23}\right). \quad (2)$$

There are some equality relations between elastic constants in tetragonal symmetries. The elastic constant C_{22} equals C_{11}, C_{23} equals C_{13}. Depending on these equations, Eq. (2) takes the following form:

$$B_0 = \frac{1}{9}\left(2C_{11} + 2C_{12} + 4C_{13} + C_{33}\right). \quad (3)$$

Using Eq. (3), the bulk modulus is easily calculated to be 133.083 GPa. It was determined that there was about 3% deviation between this bulk modulus B_0 value (133.083 GPa) and the bulk modulus B_0 value (129.008 GPa) obtained from *the Birch–Murnaghan*

TABLE III

The mechanical stability conditions, restrictions for elastic constants C_{ij} (GPa) and bulk modulus B_0 (GPa) by the crystal symmetries stability criteria in the all phases of Cu_2AlBe SMA.

Crystal symmetries of phases	Criteria for elastic constants	Restrictions for C_{ij} elastic constants	Restrictions for B bulk modulus	Refs.
Cubic ($L2_1$ phase)	$C_{11} > 0$ $C_{12} > 0$ $C_{44} > 0$	$C_{11} - C_{12} > 0$ $C_{11} + 2C_{12} > 0$	$C_{12} < B_0 < C_{11}$	[34] [35]
Tetragonal (NM phase)	$C_{11} > 0$ $C_{33} > 0$ $C_{44} > 0$ $C_{66} > 0$	$C_{11} - C_{12} > 0$ $C_{11} + C_{33} - 2C_{13} > 0$ $2C_{11} + 2C_{12}$ $+4C_{13} + C_{33} > 0$	$B_0 > \frac{1}{3}(C_{12} + 2C_{13})$ $B_0 < \frac{1}{3}(C_{12} + 2C_{33})$	[34] [36]
Orthorhombic (3M, 5M, 7M, and 9R phases)	$C_{11} > 0$ $C_{22} > 0$ $C_{33} > 0$ $C_{44} > 0$ $C_{55} > 0$ $C_{66} > 0$	$C_{11} + C_{22} - 2C_{12} > 0$ $C_{11} + C_{33} - 2C_{13} > 0$ $C_{22} + C_{33} - 2C_{23} > 0$ $C_{11} + C_{22} + C_{33} + 2C_{12}$ $+2C_{13} + 2C_{23} > 0$	$B_0 > \frac{1}{3}(C_{12} + C_{13} + C_{23})$ $B_0 < \frac{1}{3}(C_{11} + C_{22} + C_{33})$	[37] [38]

equation of state (EoS). We can interpret that in the light of these results, the martensitic tetragonal NM structure is mechanically stable.

Finally, let us focus on the mechanical stability of the newly calculated orthorhombic (3M, 5M, 7M, and 9R) phases. When we examine the elastic constants of orthorhombic phases in terms of mechanical stability criteria given in the last row of Table III, firstly, it is seen that all elastic constants calculated in our study are positive. On the other hand, it is provided also the restriction criteria given for the elastic constants C_{ij} of orthorhombic systems. The bulk modulus B_0 values for martensitic orthorhombic 3M, 5M, 7M, and 9R phases were calculated to be 126.616, 121.412, 51.637, and 52.748 GPa, respectively, from Eq. (2). As for that given in the last row of Table III, we calculated the lower limit of the bulk modulus B_0 to be 84.817, 89.700, 41.450, and 26.840 GPa for the 3M, 5M, 7M, and 9R phases, respectively. Similarly, the upper limits are calculated to be 210.213, 184.830, 72.000, and 104.570 GPa for orthorhombic martensitic phases from 3M to 9R. We can see that the elastic constants of the orthorhombic 3M and 5M phases satisfy all the stability conditions given in Table III. Moreover, the bulk modulus values for the 3M and 5M phases calculated from equation of state and elastic constants are highly compatible (deviation about 0.8% and 2%, respectively). However, even though providing the given mechanical stability requirements, the bulk modulus B_0 values of the 7M and 9R phases, which are calculated from Eq. (2), are much smaller than the values calculated from equation of state (deviation about 56%). As is known, martensitic phases according to the acoustic character of the static wave of modulation are formed by applying in order of 3-5-7-9 layer period from 3M to 9R structure [29]. The initial deformation rate of the crystal structure is increased due to the increase of the 3-5-7-9 layer periods (3M $\rightarrow$ 9R direction) in the phase modulation. Contrary to this case, the symmetry of the crystal system decreases. Thus, the elasticity of the 7M and 9R phases increases and the values of the elastic constants decrease. The bulk modulus value becomes smaller.

3.3. Electronic properties of alloys

In this subsection the influence of crystal structure on the electronic structure of Cu_2AlBe alloy is discussed. The total electronic DOS and electronic density of state of individual atoms (pDOS) from the spin-resolved bands for austenitic ($L2_1$) and martensitic (NM, 3M, 5M, 7M, and 9R) phases are determined and shown in Fig. 4a, b, Fig. 5a, b, Fig. 6a, b, respectively. When the electronic properties of the $L2_1$ structure in Fig. 4a are examined, the lowest valence bands between -10 eV and -8 eV are predominantly due to Cu $3d$ (t_{2g} and e_g) states. The majority and minority states of these bands have almost no contribution to magnetization since the DOS behavior is symmetrical. It is not seen individually that the Cu atoms contribute to the electronic state density from the s and p orbitals. Most of the contributions coming to DOS are composed of the d states of Cu atoms extending from -6 eV to 4 eV around the Fermi level. It is seen that the contributions of Al and Be atoms are considerably smaller than Cu atoms. A noticeable contribution of -6 eV to -4 eV (around -5 eV) is observed in the Cu e_g states, and this contribution decreases towards the Fermi level. In the range of -5 eV and -4 eV, a remarkably larger contribution is obtained from the Cu t_{2g} states than Cu e_g states and this contribution decreases towards -7 eV.

Above and below the Fermi level except for the range between -5 eV and -4 eV, it is seen that the contributions from the Cu e_g states are predominant.

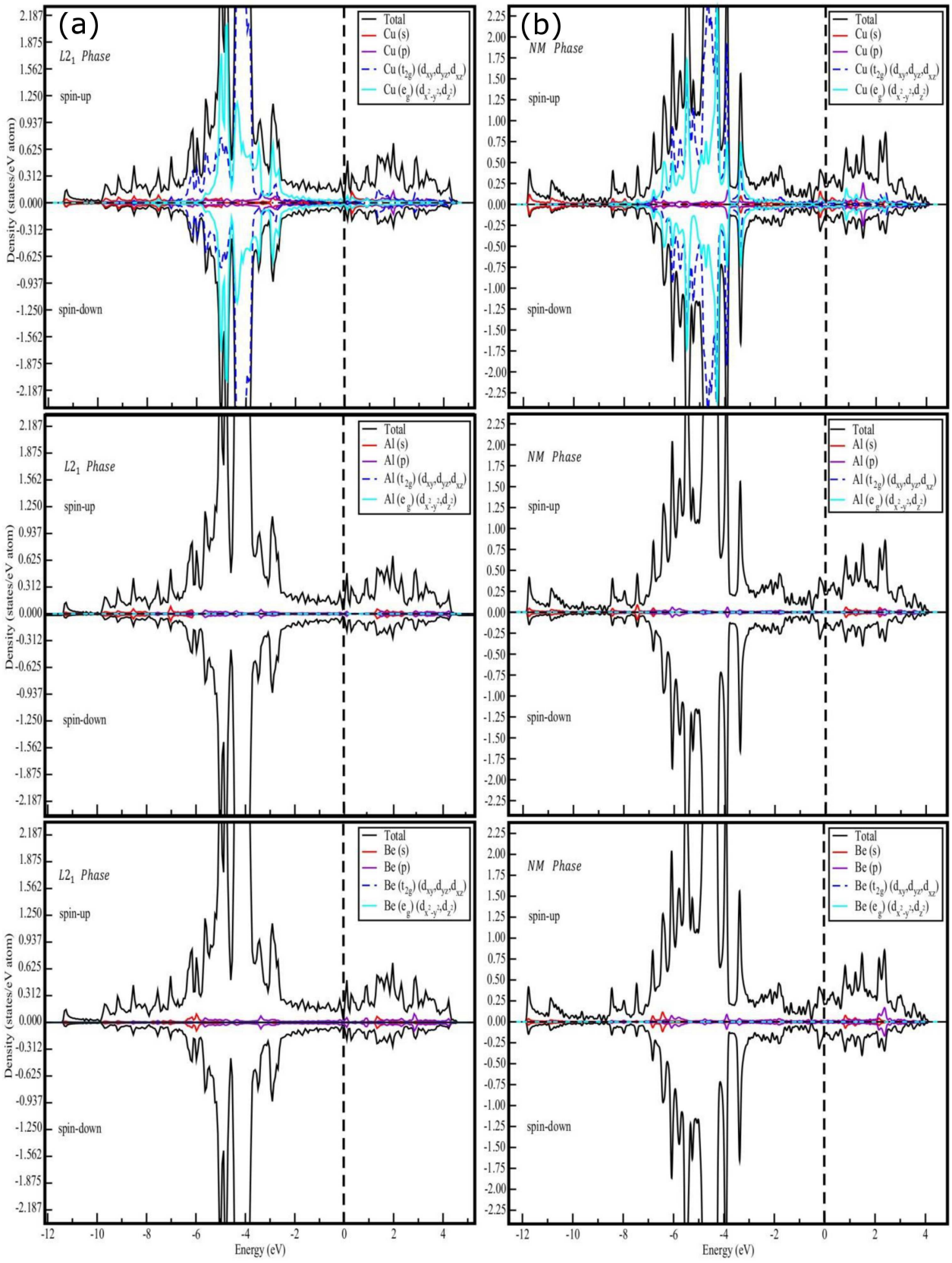

Fig. 4. Spin-up and spin-down total DOS, partial DOS for individual atoms and the decomposed t_{2g} and e_g DOS in the (a) austenitic $L2_1$ and (b) non-modulated martensitic NM structures. Vertical dot line represents the Fermi level displaced to 0 eV.

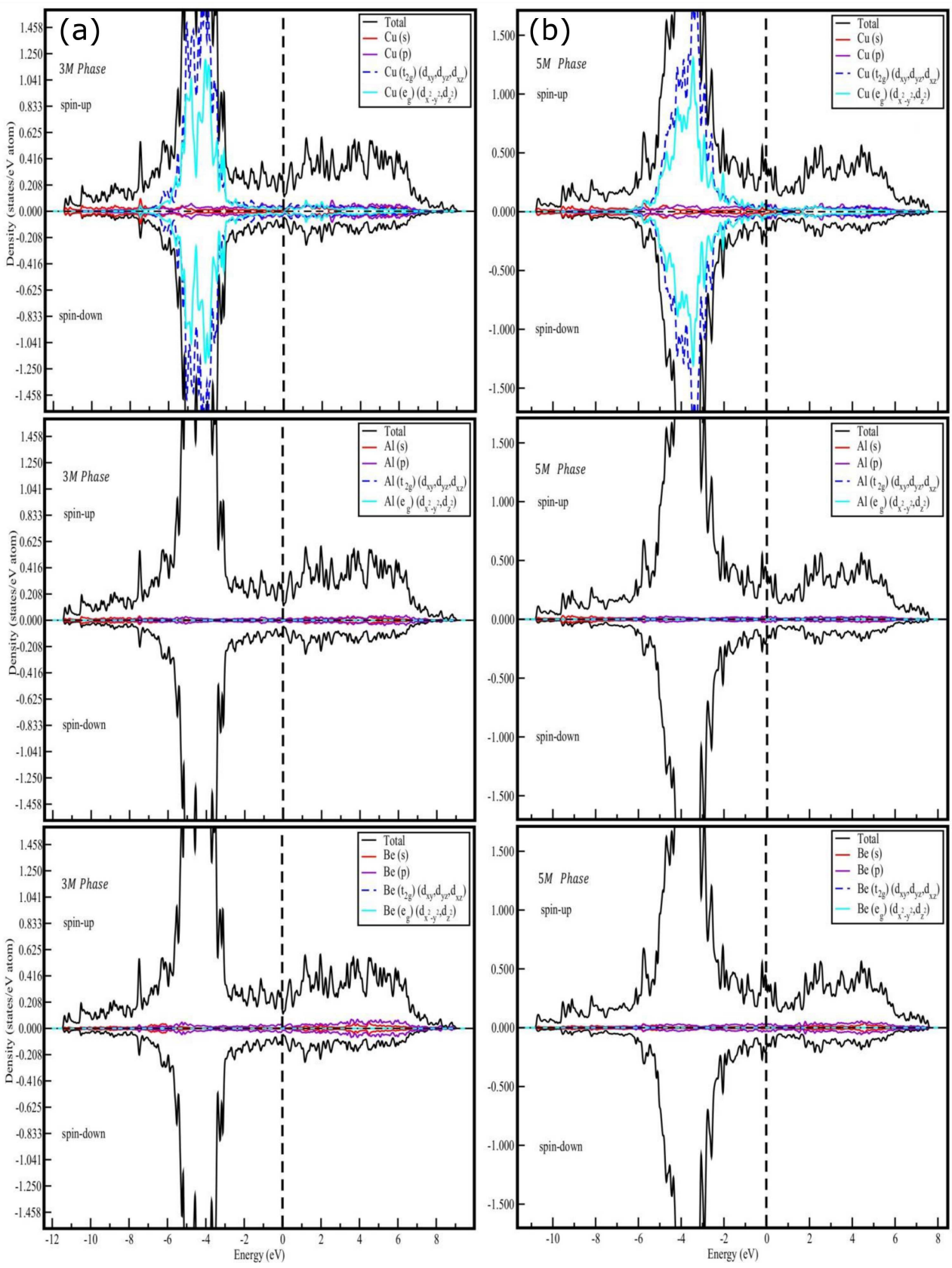

Fig. 5. Spin-up and spin-down total DOS, partial DOS for individual atoms and the decomposed t_{2g} and e_g DOS in the (a) martensitic 3M and (b) martensitic 5M structures. Vertical dot line represents the Fermi level displaced to 0 eV.

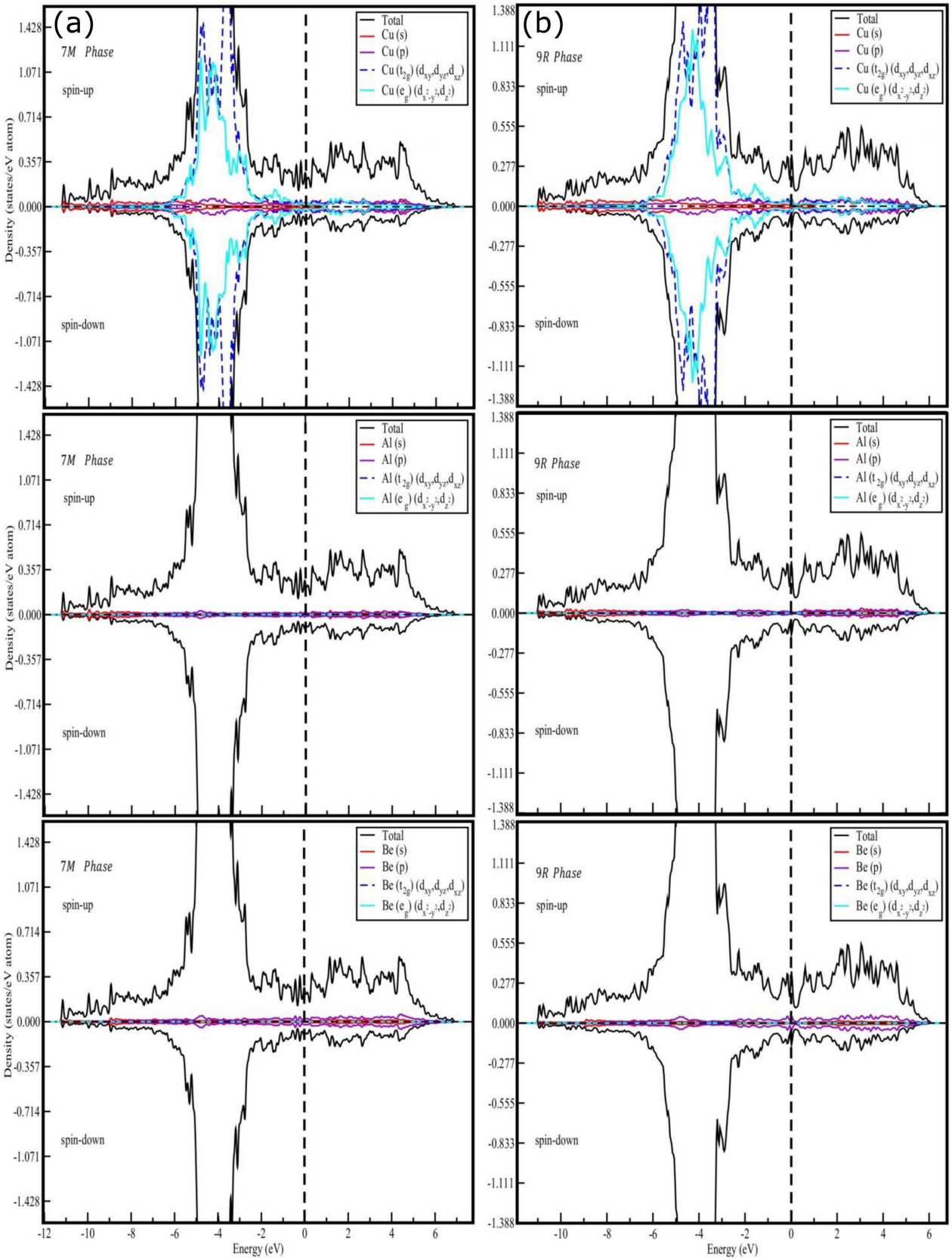

Fig. 6. Spin-up and spin-down total DOS, partial DOS for individual atoms and the decomposed t_{2g} and e_g DOS in the (a) martensitic 7M and (b) martensitic 9R structures. Vertical dot line represents the Fermi level displaced to 0 eV.

When martensitic phase transformation from the austenitic $L2_1$ to non-modulated NM martensitic phase is carried out, as shown in Fig. 4b, it is noteworthy that the contributions from the s and p orbits of Al and Be atoms are very small. Besides, there are many peaks in the range of -8 eV and -4 eV due to the contributions from both Cu t_{2g} and Cu e_g states. In the range between -7 eV and -4 eV, Cu t_{2g} states are dominant and also are similar to those to Cu e_g states. Furthermore, in the range of -4 eV to -3 eV, a peak consisting of both Cu t_{2g} and Cu e_g states is observed. A small peak occurs at about -2 eV above the level of the Fermi resulting from Cu p states. In non-modulated NM martensitic phase, it is seen that the spin-up and spin-down states are symmetrical. Accordingly, the magnetic character does not change in martensitic NM phase of the material. As one can seen in Fig. 5a, b, Fig. 6a, b, the most contribution is generally between -8 eV and the Fermi level in the martensitic 3M, 5M, 7M, and 9R phases of the material. In addition, it is seen that the contribution from t_{2g} and e_g states, which form the most contribution, changes as the phase changes. It is known that the phase shifts occurring in the materials can change the electronic properties of the material. In experimental studies, changes in the electronic structure of the Cu–Al–Be alloy in the transitions between irregular austenitic A2, regular austenitic DO_3 (or $L2_1$) and 18R martensitic phases were studied by electron energy loss spectrometry (EELS) and after the martensitic transition, the electron charge density of the material was observed to change [15]. From this point of view, in our calculations, change of distribution of electronic charge can be considered as an evidence for the presence of new phases, for transition from the austenitic to martensitic and/or between martensitic phases.

When we investigated the variation of the electron charge distribution due to the phase transitions of the Cu_2AlBe alloy, as seen in Fig. 4a and b, there is a very large peak in the $L2_1$ phase of the alloy due to Cu t_{2g} majority and minority states between -5 eV and -4 eV. As the phase transition from $L2_1$ to NM structure occurs, the intensity of the Cu t_{2g} peak is reduced and divided into two parts. One of the peaks was between -5 eV and -4 eV and the other peak was located at -4 eV. Furthermore, at the $L2_1$ phase, two sharp peaks at -5 eV were formed by Cu e_g spin-up and spin-down states. When it was passed to the NM phase, its intensity was considerably reduced and a sharp peak very close to -4 eV appeared. As shown in Fig. 5a, when it is also switched to the 3M phase, the contribution from the Cu t_{2g} states becomes quite dominant over the other phases, between -6 eV and -3 eV. This predominant contribution is present in both spin-up and spin-down states of the Cu t_{2g}. When we focus on the $L2_1$ and NM structures given in Fig. 4a and b, the intensities of 0.781 state eV/atom and 0.750 state eV/atom, respectively, observed at about -5 eV, increase dramatically to the average 1.455 state eV/atom as the material migrates to the 3M phase.

The contributions from t_{2g} states, which are distributed between -6 eV and -3 eV at 3M phase, become a sharp peak toward -3 eV energy at 5M phase. There are the two sharp peaks at -4 eV in the martensitic 7M phase. The contributions from the Cu e_g states do not change very rapidly and in large quantities during phase transitions compared to Cu t_{2g} states. In the 9R phase, no noticeable change was observed in the contributions from Cu t_{2g} and Cu e_g states. The contributions to the electronic density of state from not only s, p, t_{2g}, and e_g states of Al and Be atoms but also s and p states of Cu atom have been observed in extremely small quantity in the all austenitic and martensitic phases. As shown in Figs. 4, 5 and 6, the t_{2g} and e_g states of Cu atoms dominate in the electronic nature of the Cu_2AlBe SMA.

4. Conclusion

As shown in Fig. 3, the total energies and the lattice constants, bulk modulus B_0 GPa and its pressure derivative $B^{'}$ corresponding to different volumes per molecule of cubic $L2_1$, tetragonal NM, orthorhombic 3M, 5M, 7M, and 9R crystal structures, by fitting to a third order Birch–Murnaghan equation of state, have been calculated theoretically. The martensitic tetragonal NM phase is determined as the lowest energetic state. The phases after the NM phase as far as energies are listed as $L2_1$ →3M→ 5M →7M→ 9R, respectively. However, the energy differences between phases are compared with the thermal energy criterion $3k_BT/2$ per atom. The energy differences between the lowest energized NM phase and the phases $L2_1$, 3M, 5M, 7M, and 9R were calculated to be 0.54, 14.92, 44.47, 58.89, and 72.97 meV/atom, respectively. It has been determined that NM → $L2_1$ and NM → 3M energy differences are below the thermal energy criterion and above the energy differences of NM → 5M, NM → 7M and NM → 9R. Phases with higher energy differences than thermal fluctuation energy cannot be generated instantaneously due to thermal fluctuation. It is reasonable to assume that these phases are stable structures with minimum energy.

The calculated elastic constants, which determine the mechanical behavior of the material, are compatible with previous experimental studies [33]. The elastic constants of C_{11}, C_{12}, and C_{44} calculated by using LD show a deviation of 3%, 22%, and 6% respectively from the experimental studies. When our results obtained are evaluated, the C_{11} and C_{44} elastic constants are highly compatible with the experimental results, whereas the deviation ratio of C_{12} value is higher than the others. The second method used to calculate elastic constants is the LR method. The elastic constants of C_{11}, C_{12}, and C_{44} calculated by using LR method show a deviation of 10%, 15%, and 22% respectively from the experimental studies. There is no experimental or theoretical study to compare the elastic constants calculated for the other martensitic (NM, 3M, 5M, 7M, and 9R) phases. Accordingly, the elastic constants of five martensitic phases

(NM, 3M, 5M, 7M, and 9R) are calculated for the first time in this study. When the obtained elastic constants are evaluated in terms of mechanical stability, the elastic constants of austenitic and martensitic phases satisfy all the mechanical stability conditions given in Table III according to crystal symmetry. In addition, for the $L2_1$, NM, 3M, and 5M phases, the bulk modulus obtained not only from the equation of state, but also obtained from the mathematical relations of the elastic constants are quite compatible. However, the bulk modulus values obtained using the elastic constants given in Table III for 7M and 9R martensitic phases are found to be smaller than the bulk modulus values calculated from EoS. However, the elastic constants of these phases provide all the mechanical stability requirements given for orthorhombic crystal structures.

When the pDOS of the austenitic and martensitic phases are analyzed, it is seen that the most contribution to the electronic density of states comes from Cu t_{2g} and Cu e_g states. However, it is seen that the contributions due to the individual atoms change in phase transitions from the austenitic phase to the martensitic phase and/or between martensitic phases. This charge variation can be considered as evidence for the presence of new calculated martensitic phases (NM, 3M, 5M, and 7M) for the Cu_2AlBe alloy. However, Cu_2AlBe SMA is a non-magnetic material, since all phases of spin-up and spin-down are all symmetrical. In other words, Cu_2AlBe alloy is the conventional SMA.

Acknowledgments

Authors would like to acknowledge Ahi Evran University (BAP Project No. PYO-SAH.4001.15.001) for the support to complete this work. Computations are carried out on TUBITAK-ULAKBIM cluster. We would like to acknowledge the support of NSF-IMI at TAMU and TAMU HPCC for providing computational resources during this project. Finally, we would like to thank Prof. Dr. Tahir Cagin for critical reading of this study.

References

[1] *Shape Memory and Superelastic Alloys*, Eds. K. Yamauchi, I. Ohkata, K. Tsuchicya, S. Miyazaki, Woodhead, Cambridge 2011.

[2] J. Frenzel, E.P. George, A. Dlouhy, C. Somsen, M.F.X. Wagner, G. Eggeler, *Acta Mater.* **58**, 3444 (2010).

[3] S. Belkahla, H. Flores-Zúñiga, G. Guenin, *Mater. Sci. Eng. A* **169**, 119 (1993).

[4] R. Kainuma, S. Takahashi, K. Ishida, *Metall. Mat. Trans. A* **27**, 2187 (1996).

[5] K. Niitsu, T. Omori, R. Kainuma, *Mater. Trans. JIM* **52**, 1713 (2011).

[6] Y. Araki, N. Maekawa, T. Omori, Y. Sutou, R. Kainuma, K. Ishida, *Smart Mater. Struct.* **21**,032002 (2012).

[7] R. Amireche, M. Morin, in: *Proc. ICOMAT 2008, Santa Fe (USA)*, 2008, p. 577.

[8] M. Sade, A. Yawny, F.C. Lovey, V. Torra, *Mater. Sci. Eng. A* **528**, 7871 (2011).

[9] I. López-Ferreño, PhD. Thesis, University of the Basque Country, Bilbao 2015.

[10] H. Horikawa, S. Ichinose, K. Morii, S. Miyazaki, K. Otsuka, *Metall. Trans. A* **19**, 915 (1988).

[11] A. Ibarra, J. San Juan, E.H. Bocanegra, M.L. Nó, *Acta Mater.* **55**, 4789 (2007).

[12] M. Sade, P. La Roca, F. De Castro Bubani, F.C. Lovey, V. Torra, A. Yawny, in: *Materials Today: Proceedings* **2S**, S719 (2015).

[13] F. De Castro Bubani, M. Sade, F.C. Lovey, *Mater. Sci. Eng. A* **577**, 147 (2013).

[14] S. Montecinos, S. Tognana, W. Salgueiro, *Mater. Sci. Eng. A* **676**, 121 (2016).

[15] J.H. Hernandez, M.T. Ochoa, H. Flores-Zuniga, F. Espinosa-Magana, D. Rios-Jara, *J. Electron. Spectrosc. Relat. Phenom.***151**, 149 (2006).

[16] J. Wang, J. Li, S. Yip, *Phys. Rev. B* **52**, 12627 (1995).

[17] F. Mouhat, F.X. Coudert, *Phys. Rev. B* **90**, 224104 (2014).

[18] P. Hohenberg, W. Kohn, *Phys. Rev. B* **136**, 864 (1964).

[19] W. Kohn, L.J. Sham, *Phys. Rev. A* **140**, 1133 (1965).

[20] W. Kohn, A.D. Becke, R.G. Parr, *J. Phys. Chem.* **100**, 12974 (1996).

[21] G. Kresse, J. Furthmuller, *Comput. Mater. Sci.* **6**, 15 (1996).

[22] G. Kresse, J. Furthmuller, *Phys. Rev. B* **54**, 11169 (1996).

[23] J. Hafner, *Comput. Phys. Commun.* **177**, 6 (2007).

[24] G. Kresse, J. Hafner, *Phys. Rev. B* **47**, 558 (1993).

[25] G. Kresse, J. Hafner, *J. Phys. Condens. Matter* **6**, 8245 (1994).

[26] J.P. Perdew, K. Burke, M. Ernzerhof, *Phys. Rev. Lett.* **77**, 3865 (1996).

[27] M. Methfessel, A.T. Paxton, *Phys. Rev. B* **40**, 3616 (1989).

[28] H.J. Monkhorst, J.D. Pack, *Phys. Rev. B* **13**, 5188 (1976).

[29] A.T. Zayak, PhD. Thesis, University of Duisburg, Essen, 2015.

[30] V. Martynov, V. Kokorin, *J. Phys. III (France)* **2**, 739 (1992).

[31] Y.L. Page, P. Saxe, *Phys. Rev. B* **65**, 104104 (2002).

[32] F. Moreau, A. Tidu, P. Barbe, A. Eberhardt, J.J. Heizmann, *J. Phys. III* **5**, C2-269 (1995).

[33] S. Belkahla, Ph.D. Thesis, INSA, Lyon, France 1990.

[34] S. Piskunov, E. Heifets, R.I. Eglitis, G. Borstel, *Comput. Mater. Sci.* **29**, 165 (2004).

[35] R. Khenata, M. Sahnoun, H. Baltache, M. Rerat, A.H. Rashek, N. Illes, B. Bouhafs, *Solid State Commun.* **136**, 120 (2005).

[36] G.V. Sin'ko, *Phys. Rev. B* **77**, 104118 (2008).

[37] O. Benckstein, J.E. Klepeis, G.L.W. Hart, O. Pankratov, *Phys. Rev. B* **63**, 134112 (2001).

[38] D.C. Wallace, in: *Thermodynamics of Crystals*, Wiley, New York 1972, Ch. 1.